Fe^{2+} -catalyzed oxidative cleavages of Ca^{2+} -ATPase reveal novel features of its pumping mechanism

Cédric Montigny, Christine Jaxel, Alla Shainskaya, Joelle Vinh, Valérie Labas, Jesper V. Møller, Steven J. D. Karlish, Marc Le Maire

THE JOURNAL OF BIOLOGICAL CHEMISTRY
Vol. 279, No. 42, Issue of October 15, pp. 43971–43981, 2004
Printed in U.S.A.

Fe^{2+}-catalyzed Oxidative Cleavages of Ca^{2+}-ATPase Reveal Novel Features of Its Pumping Mechanism*

Received for publication, June 25, 2004, and in revised form, July 19, 2004
Published, JBC Papers in Press, July 19, 2004, DOI 10.1074/jbc.M407142200

Cedric Montigny‡, Christine Jaxel‡, Alla Shainskaya§, Joëlle Vinh¶, Valérie Labas¶, Jesper V. Møller‖, Steven J. D. Karlish, and Marc le Maire‡ ‡‡**

*From the ‡Unité de Recherche Associée 2096 of the Centre National de la Recherche Scientifique and Service de Biophysique des Fonctions Membranaires, Département de Biologie Joliot Curie, CEA Saclay, 91191 Gif-sur-Yvette Cedex, and Laboratoire de Recherche Associé 17V and Institut Fédératif de Recherches 46, Université Paris Sud, France, the §Biological Mass Spectrometry Facility, Weizmann Institute of Science, Rehovoth, 76100, Israel, the **Department of Biological Chemistry, Weizmann Institute of Science, Rehovoth, 76100, Israel, the ¶Laboratoire de Neurobiologie, CNRS UMR7637, Ecole Supérieure de Physique et de Chimie Industrielles, 10 rue Vauquelin, 75231 Paris cedex 05, France, and the ‖Department of Biophysics, University of Aarhus, DK-8000 Aarhus C, Denmark*

We have analyzed the Fe^{2+}-catalyzed oxidative cleavages of Ca^{2+}-ATPase in the presence of Ca^{2+}, with or without the ATP analog 5′-adenylyl-β,γ-imidodiphosphate (AMP-PNP) or in the presence of the inhibitor thapsigargin. To identify the positions of cleavages as precisely as possible, we have used previously identified proteinase K and tryptic fragments as a standard, advanced mass spectrometry techniques, as well as specific antibodies. A number of cleavages are similar to those described for Na^+,K^+-ATPase or other P-type pumps and are expected on the basis of the putative Mg^{2+} binding residues near the phosphorylated Asp^{351} in E1 or E2P conformations. However, intriguing new features have also been observed. These include a Fe^{2+} site near M3, which cannot be due to the presence of histidine residues as it was postulated in the case of Na^+,K^+-ATPase and H^+,K^+-ATPase. This site could represent a Ca^{2+} binding zone between M1 and M3, preceding Ca^{2+} occlusion within M4, 5, 6, and 8. In addition, we present evidence that, in the non-crystalline state, the N- and P-domain may approach each other, at least temporarily, in the presence of Ca^{2+} ($E1Ca_2$ conformation), whereas the presence of Mg·ATP stabilizes the N to P interaction (E1·Mg·ATP conformation).

Sarcoplasmic reticulum (SR)[1] Ca^{2+}-ATPase is a central member of the family of P-type cation-pumping ATPases (1, 2) that actively transport cations (such as Ca^{2+}, Na^+, K^+, and H^+ or even heavy metals) by a mechanism involving the formation of a phosphorylated intermediate. The Ca^{2+}-ATPase present in mature skeletal muscle, SERCA1a, contains 994 amino acid residues and has a molecular mass of 110 kDa (3). The protein has 10 trans-membrane spans M1–10 and a bulky cytosolic region, consisting of three major domains that are connected to the membrane-embedded part by a stalk. Two of these domains, the nucleotide binding domain (N) and the phosphorylation domain (P), are formed by the amino acid residues located between the membrane-spanning segments M4 and M5. The third domain (termed A) is formed from both the N-terminal tail and the amino acids located between segments M2 and M3. Recently, new structural and mechanistic information on this transport protein has been gained as a result of x-ray diffraction analysis of three-dimensional crystals of the protein (4–6). In combination with a wealth of other data obtained by site-directed mutagenesis (7, 8), by physicochemical techniques such as fluorescence with extrinsic and intrinsic (tryptophan) probes or Fourier transform infrared (*e.g.* 9, 10), and by biochemical techniques such as limited proteolysis, this has led to proposals for the actual transport mechanism for P-type ATPases (*e.g.* 11–16).

The tertiary structures of SERCA1a have been obtained by high resolution x-ray diffraction analysis of three-dimensional crystals produced from detergent-solubilized ATPase, either in the presence of Ca^{2+} ($E1Ca_2$ conformation, Ref. 4) or in the absence of Ca^{2+} but in the presence of the inhibitor thapsigargin (E2(Tg) conformation, Ref. 5). The structure revealed in Ca^{2+} (4) is very "open" with little interaction between the cytosolic domains. By contrast, a much more compact structure was obtained in the absence of Ca^{2+}, suggesting that cytosolic domains undergo large scale movements during the transition from one intermediate form to the other during catalysis (4, 5).

It is of interest that similar evidence of a compact E2 conformation accompanying active cation transport has emerged from detailed analysis of the degradation pattern, resulting from Fe^{2+}-catalyzed oxidative cleavages of Na^+,K^+-ATPase (Ref. 17 and references therein and Ref. 18) and H^+,K^+-ATPase (19). This approach has turned out to give valuable information on the location of Mg^{2+} and ATP·Mg^{2+} binding sites and also suggestive evidence on interactions between cytoplasmic domains during the enzymatic cycle. Remarkably, the proximity of some residues, far removed from each other in the linear sequence, inferred by this approach (20) has later found striking support from the three-dimensional structures of SERCA1a (4, 5) and the haloacid dehalogenase superfamily (see "Discussion" in Ref. 19). The key feature of the Fe^{2+}-catalyzed cleavage approach is that a number of peptide bonds in the immediate vicinity of bound Fe^{2+} are cleaved by the very reactive $OH^{\cdot}$

* This work was supported by the Commissariat à l'Energie Atomique/CNRS and a grant from the Israel Science Foundation 15/00-3. The costs of publication of this article were defrayed in part by the payment of page charges. This article must therefore be hereby marked "*advertisement*" in accordance with 18 U.S.C. Section 1734 solely to indicate this fact.

‡‡ To whom correspondence should be addressed. Tel.: 33-1-69086243; Fax: 33-1-69088139; E-mail: lemairem@dsvidf.cea.fr.

[1] The abbreviations used are: SR, sarcoplasmic reticulum; SERCA1a, 1a isoform of the SR Ca^{2+}-ATPase; Tg, thapsigargin; Ab, antibody; N, nucleotide binding domain; P, phosphorylating domain; A, anchor or actuator domain; AMP-PNP, 5′-adenylyl-β,γ-imidodiphosphate; Mes, 4-morpholineethanesulfonic acid; NaDOC, sodium deoxycholate; MALDI-TOF, matrix-assisted laser desorption/ionization-time of flight; Q-TOF, quadrupole-time of flight; MS, mass spectrometry; MS/MS, tandem mass spectrometry; ESI, electrospray; nanoESI, nanoscale ESI; MAP, multiple antigenic peptide.

radicals produced by the Fenton reaction. Identification of the cleavage positions reveals their proximity in the native structure. Since Fe^{2+} can replace Mg^{2+} in its binding site, near the phosphorylation site or in the Mg·ATP complex, the identification of the various cuts is thought to reflect changes in the position of the Mg^{2+} site(s) in different conformations of the pumping cycle.

In connection with these studies, the question arises as to the extent that information obtained with one ATPase type such as Na^+,K^+-ATPase, or its close relative H^+,K^+-ATPase, can be safely applied to other P-type ATPases, including SERCA, which is the only cation transporting ATPase for which a three-dimensional structure is available. However, extension of the Fe^{2+}-catalyzed cleavage approach to other P-type ATPases has been limited so far. For Ca^{2+}-ATPase, which is cleaved under these conditions (53), Hua *et al.* (21) have described Ca^{2+}- and ATP-dependent cleavages around the phosphorylation site and at Thr^{441} in the N-domain, whereas Valiakhmetov and Perlin (22) have reported ATP-dependent cleavage sites in the conserved C-terminal regions of proton ATPase. In this report, we describe in detail the Fe^{2+}-catalyzed oxidative cleavages of SERCA1a. We find that applying this procedure to SERCA1a results in a rather large number of cleavage products with a pattern that is dependent on the conformation of the enzyme. As an alternative to N-terminal sequencing to identify the cleavage positions, which is usually not feasible after oxidative cleavage, we have estimated molecular masses of fragments as precisely as possible, by comparison with a number of well known SERCA1a proteolytic fragments, by the use of mass spectrometry techniques, and with specific antibodies. From these data, it has been possible to define, with a rather high degree of certainty, how the fragments can be accounted for by cleavage at relatively few positions, in a conformation-dependent manner. A number of cuts are similar to those described previously for the other pumps, but novel features are also emerging.

MATERIALS AND METHODS

Fe^{2+}-catalyzed Oxidative Cleavage of Sarcoplasmic Reticulum Ca^{2+}-ATPase—Unless otherwise noted, all chemical products came from Sigma. SR membranes were prepared from rabbit skeletal muscle as described previously (23, 24). The membranes, stored at a protein concentration of 20–60 mg/ml, were resuspended at 0.4 mg/ml in 50 mM Tris, pH 7.2, and 50 mM KCl either (i) with no Ca^{2+} added or (ii) with the addition of 0.1 mM Ca^{2+} or (iii) incubated with 50 μM thapsigargin (added to the suspension from a 1 mM thapsigargin stock solution in Me_2SO). At pH 7.2, both the first and second condition stabilize the Ca^{2+}-ATPase in an E1 conformation since the level of contaminating Ca^{2+} ($\sim$10 μM) is sufficient to saturate the high affinity binding sites of Ca^{2+}-ATPase, whereas the third condition (the addition of thapsigargin) stabilizes the Ca^{2+}-ATPase in an E2(Tg) conformation (25). Experiments were also performed at a lower pH, in a buffer containing 50 mM Mes, pH 5.5, 50 mM KCl, with or without the addition of 0.1 mM Ca^{2+} or 50 μM thapsigargin. The rationale for using pH 5.5 was, as suggested from previous findings (26), to bring the ATPase into an E2 conformation without the addition of thapsigargin or EGTA; the use of the latter in the present experiments is problematic since it chelates Fe^{2+} with an even higher affinity than Ca^{2+}. Indirect evidence that, at pH 5.5 without added Ca^{2+}, the ATPase is indeed present mainly in an E2 conformation was obtained from enzyme activity measurements. Whereas at pH 7.2, the ATPase was fully activated in the absence of added Ca^{2+}, relative to that measured spectrophotometrically at 0.1 mM Ca^{2+} (27), at pH 5.5, only 15% activation was observed.

In the standard procedure for producing Fe^{2+}-catalyzed fragments of Ca^{2+}-ATPase by oxidative cleavage, we first incubated the membrane suspensions for 5 min at 4 °C with 10 μM $FeSO_4$, added from a freshly prepared $FeSO_4$ stock solution (1 mM), and then for 2 min at 20 °C before initiating the cleavage reaction by the addition of ascorbate/H_2O_2 at final concentrations of 5 or 10 mM ascorbate and 9 mM H_2O_2. The ascorbate and H_2O_2 were added from stock solutions of freshly prepared 200 mM ascorbic acid, 200 mM Tris (pH 7.2) or 200 mM ascorbic acid, 200 mM Mes (pH 5.5) and 90 mM hydrogen peroxide. After 5–60 min (usually 10 min), the reaction was stopped by the addition of EDTA and deferoxamine (Sigma) at final concentrations of 20 and 4 mM, respectively. The membrane suspensions were chilled at 0 °C before the addition of equal volumes of a 2-fold concentrated gel sample buffer (0.1 M Tris/HCl, pH 8, 4% SDS, 5 mM EDTA, 1.4 M β-mercaptoethanol, 8 M urea, and 0.025% bromphenol blue). After heating for 1 min at 100 °C, the samples were cooled for 5 min at room temperature before loading onto 10% 7 × 9 cm Laemmli gels, which were stained with Coomassie Blue or electroblotted onto polyvinylidene difluoride paper for Western blot analysis. For mass spectroscopy, samples were prepared as described above but with the following modifications. When the Fe^{2+}-cleaved fragments were to be analyzed after extensive trypsinization, gels were first immersed for 10 min in a Coomassie Blue staining solution (40% methanol, 10% acetic acid, 0.1% Coomassie Blue R250) and destained with 10% methanol, 10% acetic acid, 1% glycerol until the bands could be seen. The bands were then excised onto a clean glass plate and stored in tubes with some acetic acid at 4 °C before trypsinization and mass spectrometry analysis (MALDI-TOF MS and nanoscale electrospray (nanoESI)-quadrupole-time of flight (Q-TOF) tandem mass spectrometry (MS/MS)). The protein bands were in gel reduced and alkylated by dithiothreitol and iodoacetamide, respectively, before overnight enzymatic digestion with trypsin as described previously (28). When intact iron-cleaved fragments were to be analyzed, the iron cleavage incubation time was increased to 40 min to accumulate a maximum amount of the different fragments. After the cleavage reactions, the samples were centrifuged 15 min at $\sim$20000 × *g* on an MR22i JOUAN centrifuge at 4 °C. The membrane pellets were resuspended in 20 μl of buffer (50 mM Tris, pH 7.2, 50 mM KCl or 50 mM Mes, pH 5.5, 50 mM KCl) and kept at 0 °C until the addition of equal volumes of a 2-fold concentrated gel sample buffer (0.1 M Tris/HCl, pH 8, 4% SDS, 5 mM EDTA, 1.4 M β-mercaptoethanol, 8 M urea, and 0.025% bromphenol blue). After heating for 1 min at 100 °C, the samples were left for 5 min at room temperature before loading onto 10% 16 × 16 cm Laemmli gels. Each lane contained about 80 μg/40 μl protein with 1 mM thioglycolate acid added to the cathode buffer. Depending on the type of mass spectrometry analysis, the gels were then processed differently. For analysis of the intact bands, the gel was stained over a period of 20 min in a GelCode solution (Perbio, Bezons, France) and destained in Millipore-filtrated water until the bands became visible. The bands were excised from the gel on a clean glass plate and kept at 4 °C. In another series of experiments, the intact fragments were examined by mass spectroscopy after blocking their sulfhydryl groups with iodoacetamide (see Table II, *with alkylation*). In that case, the samples were cleaved and centrifuged as before, but after centrifugation, the membrane pellets were suspended in 200 μl of a 100 mM sodium acetate, pH 4.5, 0.5% SDS, 50 mM dithiothreitol and were incubated for 60 min at room temperature. Iodoacetamide was then added at a final concentration of 250 mM, and the tubes were incubated for an additional 60 min at room temperature. Proteins were precipitated overnight at −20 °C by the addition of 4 volumes of a 2:1 methanol:ether solution.

Fe^{2+}-catalyzed Oxidative Cleavage of Renal Na^+,K^+-ATPase—Pig kidney Na^+,K^+-ATPase was prepared as described (29). Oxidative cleavage of renal Na^+,K^+-ATPase catalyzed by Fe^{2+} ions or the ATP·Fe^{2+} complex was performed essentially as described previously (20, 30, 31). For preparation of samples to be analyzed by MALDI-TOF MS, $\sim$3 mg of Na^+,K^+-ATPase was cleaved in one of the following conformational states. E2(Rb)·Fe^{2+} or E1Na·Fe^{2+} enzyme was suspended in media containing 10 mM Tris HCl, pH 7.4, 20 mM RbCl (or 20 mM NaCl) and incubated for 10 min at room temperature with 1 μM $FeSO_4$, 5 mM ascorbate, 5 mM H_2O_2; E1·ATP·Fe^{2+}; the enzyme was suspended in a medium containing 50 μM AMP-PNP, 250 mM NaCl, 10 mM TrisHCl, pH 7.4, and incubated at room temperature for 30 min with 5 μM $FeSO_4$, 5 mM ascorbate, 5 mM H_2O_2; E2P·Fe^{2+} (see Table II): the enzyme was incubated with 130 mM NaCl, 1 mM ATP, and 50 μM $FeSO_4$ for 2 min at 0 °C; 1 mM ouabain was then added, and after 1 min, 4 mM deferoxamine (Sigma), 20 mM ascorbate, and 20 mM H_2O_2 were added, and the suspension was incubated for a further 4 min. At the end of each incubation, the cleavage reactions were arrested by the addition of 10 mM deferoxamine, 10 mM EDTA, and the membranes were collected by centrifugation and resuspended in a medium containing 25 mM imidazole, 1 mM EDTA, and 10 mM RbCl. The enzyme (0.5 mg/ml) was then solubilized with an equal volume of the non-ionic detergent $C_{12}E_{10}$ (1.5 mg/ml), and undissolved protein was removed by centrifugation. Protein was further precipitated from the detergent solution by the addition of 4 volumes of methanol:ether 3:1 (v:v) overnight at −20 °C and collected by centrifugation. The precipitated protein was dissolved in 0.5% SDS, applied to a TSK-3000 size exclusion high

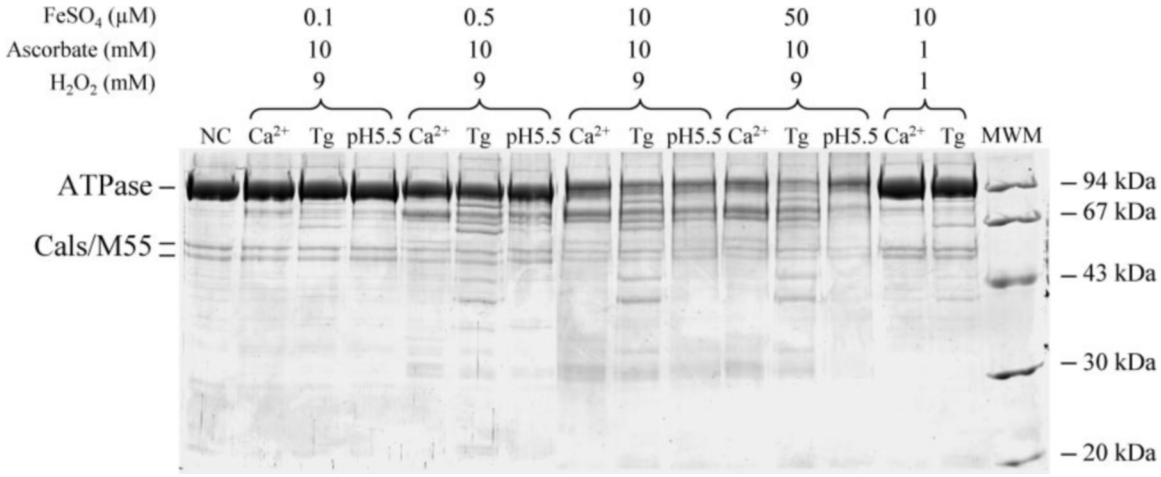

FIG. 1. **Effect of Fe^{2+} concentration on of SERCA1a proteolysis.** SR membranes (0.4 mg/ml) were proteolyzed by incubation for 10 min with ascorbate/H_2O_2 and various concentrations of Fe^{2+}, as indicated on *top* of the figure. The incubation media were 50 mM Tris, pH 7.2, 50 mM KCl, 0.1 mM Ca^{2+} (indicated as *Ca*$^{2+}$ on *top* of the gel, E1 conformation) or 50 mM Tris, pH 7.2, 50 mM KCl, 50 μM thapsigargin (indicated as *Tg* on *top* of the gel, E2 conformation) or 50 mM Mes, pH 5.5, 50 mM KCl, with no Ca^{2+} added (indicated as *pH 5.5* on *top* of the gel, E2 conformation). About 3.8 μg of Ca^{2+}-ATPase was loaded in each lane on a 10% Laemmli gel. Coomassie Blue staining is shown. *Cals/M55*, calsequestrin and the M55 glycoprotein; *NC*, non-cut (control SR); *MSM*, molecular size markers.

pressure liquid chromatography column, and eluted with a solution of 100 mM sodium acetate, pH 4.5, 0.1% SDS (32). 50 mM dithiothreitol was added to each fraction, and after an overnight incubation at 4 °C, solid iodoacetamide was added to 250 mM and incubated for 1 h at room temperature, and then 50 mM dithiothreitol was added to quench the excess of iodoacetamide. The protein was precipitated again with 4 volumes of methanol:ether and collected. Protein was dissolved in 5-fold concentrated gel sample buffer with 5 mM EDTA added. Fragments were separated on long 10% Tricine-SDS gels, which were stained with Coomassie Brilliant Blue and/or colloidal stain GelCode (Pierce).

Preparation of Cleavage Fragments for Intact Mass Measurements by MALDI-TOF Mass Spectrometry, Electroelution of Protein, and Exchange of SDS by Deoxycholate—Electroelution of protein from pieces of the SDS-gels was performed in GeBAflex-tubes (Gene Bio Application Ltd., Kfar Hanagid, Israel) at 150 V for 2 h (see Ref. 33). The elution buffer contained 0.025% SDS, 25 mM Tris, and 250 mM Tricine, pH 8.5. Following electroelution, SDS was efficiently removed by precipitating the protein solution with 50% trichloracetic acid in the presence of 0.5% sodium deoxycholate (NaDOC) for 15 min at room temperature. After centrifugation, the pellets were resuspended in the cold acetone and centrifuged again after overnight incubation at −20 °C to remove traces of unbound NaDOC, and samples were subjected to mass spectrometric analysis. Acetone can also be replaced by methanol. Estimation of the protein recovery was performed by densitometric analysis.

MALDI-TOF-Mass Spectrometry of Whole Fragments—Aliquots of the electroeluted proteins dissolved in 80% formic acid, followed by dilution to a final concentration of 10% formic acid and immediate sonication for 5 min at 30 °C, were used for MALDI-TOF MS by using dry droplet (34) methods. 2,5-dihydroxybenzoic was used as matrixes for analysis. Mass spectrometric analysis was performed on a Bruker Reflex III™ MALDI-TOF mass spectrometer (Bruker, Bremen, Germany), equipped with a delayed extraction ion source, a reflector, and a 337-nm nitrogen laser.

Analysis of Protein Digests by MALDI-TOF MS and nanoESI-Q-TOF MS and MS/MS—The tryptic digests were analyzed first in reflector mode on an Applied Biosystems STR MALDI TOF mass spectrometer (Applera, Framingham, MA) equipped with a delayed extraction ion source and a 337-nm N_2 laser to generate a peptide mass fingerprint, and then they were analyzed by nanoESI MS/MS using a hybrid nanoESI quadrupole-time of flight mass spectrometer (Q-Tof2, Waters, Micromass, Manchester, UK) in direct infusion mode with metal-coated glass capillaries (Proxeon, Odense, Denmark). In automatic mode, data acquisition was realized by switching between the survey acquisition in MS mode and fragmentation acquisition in MS/MS mode on the four most intense ions detected in the former survey scan and using dynamic exclusion afterward. Mass data collected during an analysis were processed and converted into a pkl file using the Masslynx™ software (Micromass) to be submitted to the search software Mascot (www.matrixscience.com). Protein identifications were obtained by comparison of experimental data with the NCBInr data base. In manual mode, bi- or tri-protonated precursors were selected for fragmentation and were manually processed using the Peptide Sequencing software (Masslynx™, Waters).

Other Methods—ATPase activities were measured at 23 °C with an ATP generating system (27) in 50 mM Mes (pH adjusted to 5.5, 6, or 7 with NaOH), 50 mM KCl, 5 mM Mg·ATP, and 5 mM Mg^{2+}, without or with 0.1 mM added Ca^{2+}. For estimation of molecular masses, the electrophoretic mobility of the Fe^{2+}-cleaved fragments was compared with that of well known proteolytic cleavage products (35), obtained by treating Ca^{2+}-ATPase (1 mg of protein/ml) with proteinase K (0.03 mg/ml) for 5 min at 20 °C in a 50 mM Bis-Tris, pH 6.5, 50 mM NaCl, 10 mM $MgCl_2$, and 1 mM EGTA buffer. Tryptic peptides were obtained by treating Ca^{2+}-ATPase (2 mg protein/ml) with trypsin (0.04 mg/ml) for 5–120 min at 20 °C in a buffer containing 50 mM Mes-Tris, pH 6, 50 mM NaCl, and either 2 mM EGTA or 0.1 mM Ca^{2+}. The reaction was stopped by trypsin inhibitor (0.1 mg/ml) and phenylmethylsulfonyl fluoride (2 mM) as described previously (36). Western blotting was performed as described (35). SERCA rabbit polyclonal sequence-specific antibodies 577–588 and 985–994 were prepared against the corresponding peptides coupled to keyhole limpet hemocyanin as described previously (35, 37), whereas N-terminal antibody MAP 1–15 was prepared without coupling to keyhole limpet hemocyanin by a multiple antigenic ("dendritic") peptide (38) corresponding to the 15 N-terminal amino acids of the SERCA1a protein (Research Genetics). The Na^+,K^+-ATPase C-terminal antibody anti-KETYY was described previously (32).

RESULTS

Fe^{2+}-catalyzed Oxidative Cleavage—Fig. 1 shows the effect of a wide range of Fe^{2+} concentrations on the oxidative cleavage of Ca^{2+}-ATPase in the presence of ascorbate and H_2O_2. As can be seen, many bands appear on the Coomassie Blue-stained gel, particularly in the E2 conformation induced by the addition of thapsigargin (Tg). Extensive cleavage is observed at 10–50 μM Fe^{2+}, but it is also possible to induce cleavage at very low Fe^{2+} concentrations. Thus, fragments are already visible at 0.5 μM Fe^{2+} provided that ascorbate and H_2O_2 are not below a concentration of about 10 mM. At the protein concentration used in these experiments, the Ca^{2+}-ATPase is present at about 3 μM; thus, the Fe^{2+}/Ca^{2+}-ATPase molar ratio is low, suggesting that the fragments are the consequence of the binding of a few specifically located Fe^{2+} ions. The cleavage at pH 5.5 is slightly more extensive, but the pattern resembles that at pH 7.2. The two extrinsic proteins, calsequestrin and M55, remain essentially unaffected by the cleavage conditions except at very high Fe^{2+} concentrations and low pH. We have explored further the nature of the cleavage products with the aid of sequence-specific antibodies: one directed to the N terminus

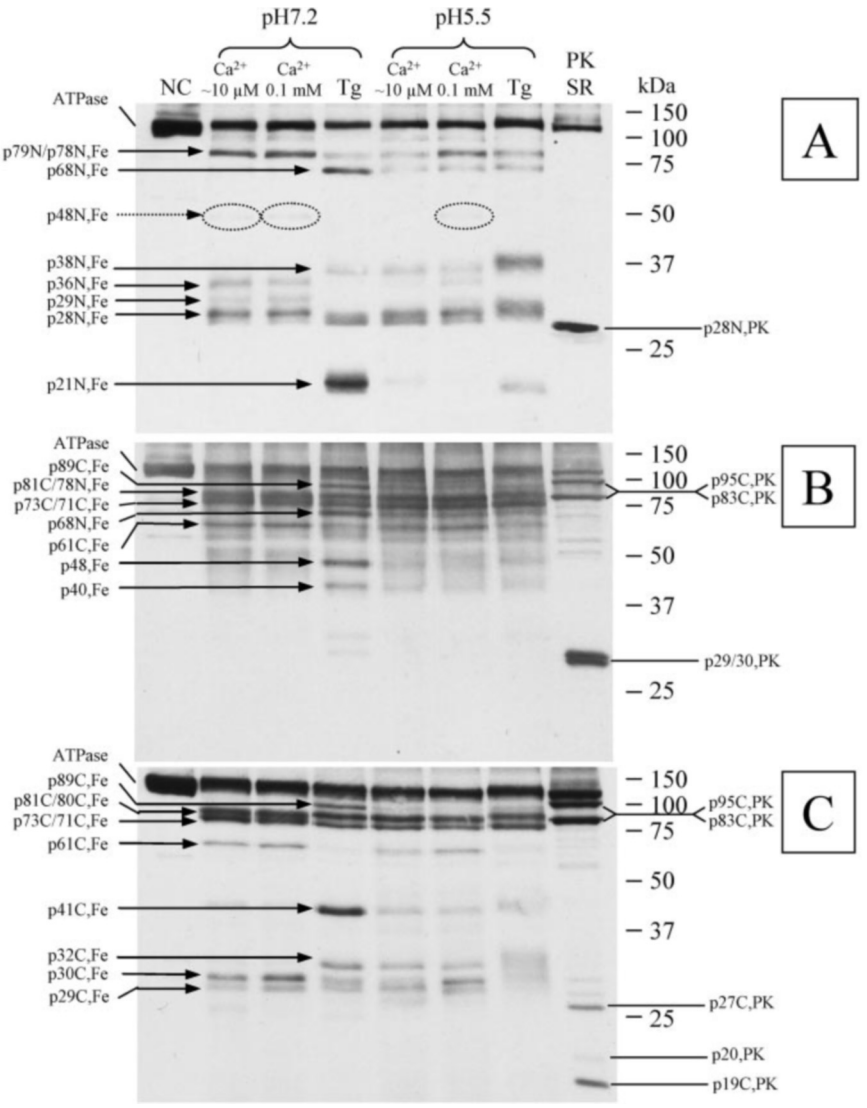

FIG. 2. **Fe^{2+}-oxidative cleavage revealed by Western blots.** SR membranes (0.4 mg/ml) were proteolyzed by the addition of 10 μM Fe^{2+} and incubated for 10 min with 10 mM ascorbate, 9 mM H_2O_2. The incubation media were: in the *left part of the blot*, 50 mM Tris, pH 7.2, 50 mM KCl, with either no Ca^{2+} added (indicated as *~10 μM Ca^{2+}* on *top* of the blot, E1 conformation) 0.1 mM Ca^{2+} (as indicated on *top* of the blot, E1 conformation), or 50 μM thapsigargin (indicated as *Tg* on *top* of the blot, E2 conformation), or in the *right part of the blot,* 50 mM Mes, pH 5.5, 50 mM KCl, with no Ca^{2+} added (indicated as *~10 μM Ca^{2+}* on *top* of the gel, E2 conformation), 0.1 mM Ca^{2+} (as indicated on *top* of the gel, E1 conformation), or 50 μM thapsigargin (indicated as *Tg* on *top* of the blot, E2 conformation). About 1 μg of Ca^{2+}-ATPase was loaded in each lane on a 10% Laemmli gel. After transfer to polyvinylidene difluoride membranes, the blots were revealed using antibodies Ab MAP 1–15 against the N terminus (*A*), Ab 577-88 against the central part (*B*), and Ab 985-94 against the C terminus (*C*), all of them at a dilution of 3000×. The ECL system (Amersham Biosciences) was used, and the films were exposed about 2 min. The last lane on the *right*, before the prestained standard, contained SR vesicles cleaved with proteinase K (*PK SR*) in the presence of EGTA as described under "Materials and Methods." The peptides are labeled as described previously (35), based on their apparent mass (those produced by cleavage with Fe^{2+} or proteinase K), *N* or *C* indicating whether the peptide contains the N or the C terminus of the protein based on the Western blots (see Table I to locate them in the SERCA1a sequence). *NC*, non-cut (control SR).

(antibody MAP 1–15), one to the C terminus (antibody 985–994), and one to a sequence near the middle of the ATPase polypeptide chain (antibody 577–588). Fig. 2, *A–C*, presents Western blots obtained with these antibodies in the presence or absence of added Ca^{2+} or of Tg. Although the data are complex, close examination shows that they are amenable to detailed analysis. As a first observation, we note that most of the bands on the blots are present as complementary pairs, *e.g.* as heavily stained bands p68N/p41C, p21N/p89C (lane labeled *pH 7.2*, *Tg*) and p79N/p30C (lane labeled *pH 7.2*, *0.1 mM Ca^{2+}*). The sum of these fragments adds up to that of uncleaved ATPase, which is as expected since, according to previous experience, oxidative cleavage results in each polypeptide chain being cut only once (20). However, there appear to be exceptions to this rule since the use of Ab 577-588 provides unambiguous evidence for the presence of peptides that react neither with the N-terminal nor with the C-terminal antibody (p40 and p48), and these peptides must therefore be derived from doubly cleaved ATPase. A comparison of the fragmentation pattern in the different lanes leads to the following conclusions. 1) At pH 7.2, the principal Ca^{2+}-specific bands are p79N, p30C, p61C, and p36N, which are present together with a number of less prominent N-terminal and C-terminal bands at p30N and p29C. All bands formed at 10 μM Ca^{2+} and 0.1 mM Ca^{2+} at pH 7.2 are present in nearly equal amounts, in accordance with Ca^{2+}-ATPase being present in the same E1 conformation. 2) In the presence of Tg at pH 7.2, the most intense bands are p21N/p89C, p68N/p41C, p32C, p40, and p48, all of which originate from cleavage in the cytosolic domain and are probably related to the processes by which the ATPase is dephosphorylated (see below). 3) At pH 5.5, the degradation pattern in the presence of Ca^{2+} resembles that at pH 7.2, but N-terminal bands tend to be weaker at 10 μM Ca^{2+} (in which the ATPase approaches an E2 conformation, cf. "Materials and Methods"). At this pH, the effect of Tg also tends to be less distinct except for an abundant formation of p38N originating from cleavage at the phosphorylation site (see below). 4) Subsidiary bands (p28N/p29N, originating from the membrane interface sector) are formed in about equal amounts at pH 7.2 and 5.5 in the presence or absence of Tg. The above conclusions, based on the antibody data, were corroborated by the Coomassie Blue-stained gel (data not shown).

In a number of additional experiments, we explored the effect of variations of the incubation time and of the concentrations of Fe^{2+} and ascorbate. In general, these experiments demonstrated, as expected, the simultaneous emergence of complementary bands. Furthermore, the use of gels with a lower acrylamide content enabled a better resolution of peptides with high molecular masses than observed in Fig. 2. Fig. 3 shows a direct comparison of the cleavage pattern of Ca^{2+}-ATPase and Na^+,K^+-ATPase analyzed by Western blots, using C-terminal antibodies against both ATPases. Given that the condition in Rb^+ for Na^+,K^+-ATPase corresponds to the E2

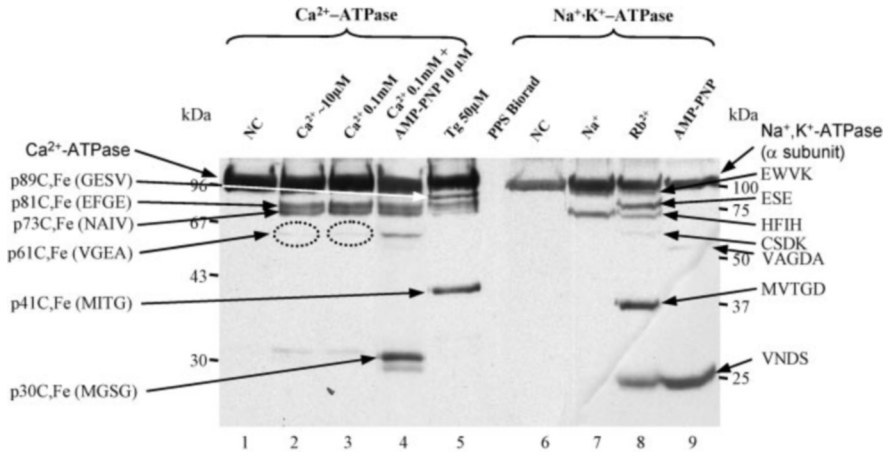

FIG. 3. **Comparison of Fe^{2+}-oxidative cleavage of Ca^{2+}-ATPase and Na^+,K^+-ATPase revealed by Western blots.** Cleavage conditions for Ca^{2+}-ATPase were the same as in Fig. 2 (pH 7.2 buffer). In *lane 4*, the medium contained 10 μM AMP-PNP in addition to 0.1 mM Ca^{2+}. Ab 985-994 was used as in Fig. 2. Samples of cleaved renal Na^+,K^+-ATPase were produced as in Fig. 1 of Patchornik *et al.* (43), and the incubation medium contained NaCl (*lane 7*), RbCl (*lane 8*), or NaCl and AMP-PNP (*lane 9*). Ab anti-KETYY (dilution 3000×) was used to reveal *lanes 6–9* (exposure time 2 min). *NC*, non-cut (control SR); *PPS*, prestained standard.

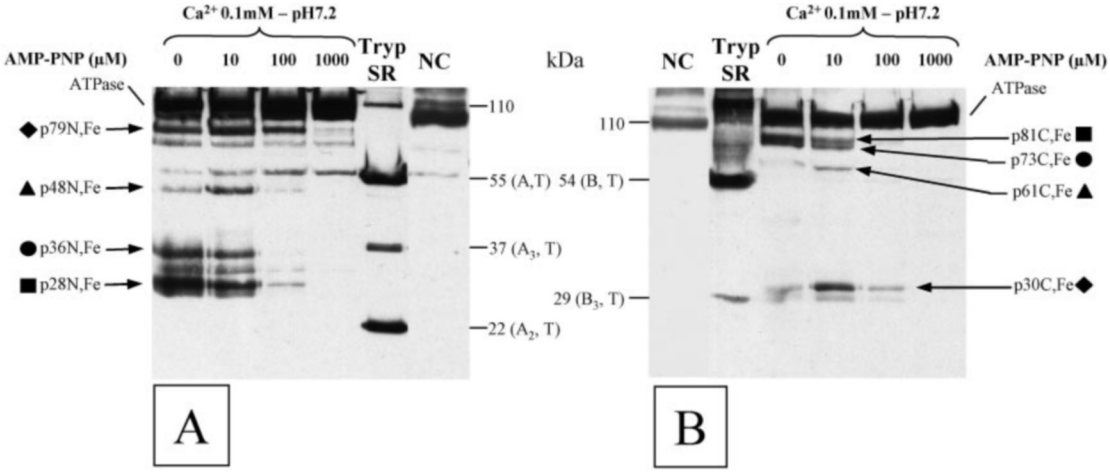

FIG. 4. **Effect of increasing concentrations of AMP-PNP on Fe^{2+}-oxidative cleavage of Ca^{2+}-ATPase as revealed by Western blots using N-terminal (*A*) or C-terminal antibodies (*B*).** The conditions of cleavage were the same as in Fig. 3 except that increasing concentrations of AMP-PNP were used, as indicated on *top* of the lanes. Ab MAP 1–15 (*A*) or Ab 985-994 (*B*) both diluted 3000 times were used as in Fig. 2, but the films were exposed for a longer period (10 min). The lane labeled *Tryp SR* contained SR vesicles cleaved with trypsin as described under "Materials and Methods" so that the peptides formed could be used as intrinsic markers of molecular mass (see Table I for the identification of these peptides). *NC*, non-cut (control SR).

conformation for Ca^{2+}-ATPase after thapsigargin binding, whereas the addition of Na^+ for Na^+,K^+-ATPase corresponds to the E1 conformation for Ca^{2+}-ATPase in the presence of Ca^{2+}, the figure demonstrates a basic similarity between the oxidative cleavage pattern of the two ATPases. This is also the case after binding of nucleotide (AMP-PNP). Fig. 4 shows in more detail the effect of AMP-PNP addition on Ca^{2+}-ATPase; it is seen that at a low concentration of AMP-PNP (10 μM), there is an increase in the formation of the complementary p79N/p30C and p48N/p61C bands, accompanied by a reduced formation of p36N/p73C and p28N/p81C. Higher concentrations of nucleotide (100 μM and 1 mM), on the other hand, result in a marked decrease or disappearance of all fragment. As described previously for Na^+,K^+-ATPase (31), these are the features expected for a nucleotide·Fe^{2+} complex acting as an affinity cleavage reagent at the lower nucleotide concentration and by competitive displacement of the nucleotide·Fe^{2+}complex from Ca^{2+}-ATPase by uncomplexed AMP-PNP at the high concentrations. Furthermore, the reduction in the intensity of fragments produced by bound Fe^{2+} without nucleotide (p36N/p73C and p28N/p81C) may be considered to be due to chelation of Fe^{2+} by the added nucleotide, thereby reducing binding to the Fe^{2+} sites (Table I).

A summary of the data is presented in Table I, which shows tentative assignments of peptides based on cleavage points deduced from: 1) apparent molecular masses on SDS-PAGE calibrated with molecular masses markers and with well identified proteinase K and tryptic peptides and 2) Western blots with three different sequence-specific antibodies (such as the ones shown in Figs. 2 and 3) by comparison with proposed Fe^{2+}-induced cleavage sites of the Na^+,K^+-ATPase and H^+,K^+-ATPase, as described in Table I of Shin *et al.* (19). The site designations (sites I and II) are also taken from this table, whereas the domain designation is based on the Ca^{2+}-ATPase structural model (4, 5). In accordance with the previous studies, the cleavage pattern is thus interpreted in terms of two separate Fe^{2+} binding sites, site I being located in the cytosolic domain and site II being located in the membrane interface region. It can be seen that according to this analysis, site I cleavages are strongly conformation-dependent, whereas this is hardly the case for cleavages at site II. Most of the previously identified cleavage positions for Na^+,K^+-ATPase and H^+,K^+-

TABLE I

Location and masses of cleavage fragments of Ca^{2+}-ATPase based on the results obtained on Na^+,K^+-ATPase and H^+,K^+-ATPase and on formerly identified proteinase K and trypsin fragments of the Ca^{2+}-ATPase

Proteinase K fragments are defined in Ref. 35, and the trypsin fragments are defined in Refs. 51 and 52.

Tentative assignments	Name of fragment	Site and domain	Conditions	Theoretical mass
				kDa
^{182}GESVSV . . .	p89C	Site I A	Tg 50 μM pH 7.2, major (minor at pH 5.5)	89.1
	p21N			20.5
^{255}EFGEQLS . . .	p81C	Site II	All conditions, major	81.4
	p28N	membrane		28.2
^{260}LSKVI . . .	p80C	Site II	Ca^{2+} 10 μM or 0.1 mM pH 7.2 (minor)	80.2
	p29N	membrane		29.2
^{731}SEMV . . .	p80N	Site I P	All conditions (minor)	79.9
	p29C			29.5
^{720}MGSG . . .	p79N	Site Ia P	Ca^{2+} 10 μM or 0.1 mM pH 7.2	79.0
	p30C		and Ca^{2+} 0.1 mM pH 5.5 (minor in Tg); increased in 10 μM AMP-PNP	30.5
^{703}DGVNDA . . .	p78N	Site I P	Tg 50 μM pH 7.2	77.3
	p32C		(and all conditions at pH 5.5: minor)	32.1
^{330}NAIV . . .	p73C	Site I P	Ca^{2+} 10 μM or 0.1 mM pH 7.2	73.2
	p36N			36.2
^{351}DKTGT . . .	p71C	Site I P	Tg 50 μM pH 7.2 and all conditions at pH	71.2
	p38N		5.5 (minor)	38.3
^{623}MITG . . .	p68N	Site I P	Tg 50 μM pH 7.2, major	68.4
	p41C		(and all conditions at pH 5.5: minor)	41.1
^{437}VGEATET . . .	p61C	Site Ia N	Ca^{2+} 10 μM or 0.1 mM at pH 7.2 and 5.5	61.8
	p48N		(minor in Tg) increased in 10 μM AMP-PNP	47.6
^{182}GESV(. . .)IRVI^{622}	p48	Site I A and P	Tg 50 μM pH 7.2, major	48.1
	p21N			20.5
^{623}MITG . . .	p41C			41.1
^{255}EFGEQLS(. . .)IRVI^{622}	p40	Site I and II	Tg 50 μM pH 7.2	40.3
^{623}MITG . . .	P28N	membrane		28.2
	p41C	and P		41.1
^{120}KEY . . .	p95C		Proteinase K	96.1
^{243}EQDKT . . .	p83C			82.8
^{350}DKTG(. . .)MGSI^{611}	p29/30			~29
^{1}M(. . .)QMAAT^{242}	p28N			26.6
^{747}VEEG . . .	p27C			27.8
^{808}GFNPP . . .	p19C			20.1
^{1}M(. . .)SSR^{505}	A		Trypsin	55.4
^{506}AAV . . .	B			54.0
^{1}M(. . .)DPR^{198}	A_2			22.1
M1(. . .)IVR^{334}	A_3			36.6
^{729}TAS . . .	B_3			29.7

ATPase are also found in the Ca^{2+}-ATPase, but there are also a few additional cuts, particularly at site II near residue 260 in trans-membrane segment M3 or in site I near residues 330 and 720 in the P-domain (observed only in Ca^{2+}), whereas a new (minor) cut near 730 at the end of the P-domain is observed in both Ca^{2+} and Tg. On the other hand, we could not identify with certainty the cleavage near the residue 48 (at the entrance to trans-membrane segment M1), expected to be present on the basis of observations with Na^+,K^+-ATPase (19). The location of the cleavage sites is also shown on a linear map of the ATPase polypeptide chain in Fig. 5, with an indication of which cleavages are related to site I and to site II, respectively, and which cleavages are increased by nucleotide binding (*site Ia*).

Validation of Cleavage Sites by Mass Spectroscopy—All attempts to define cleavage sites of Ca^{2+}-ATPase by N-terminal sequencing were unsuccessful because oxidative cleavages ordinarily do not produce free N termini of the fragments, thus precluding Edman degradation (39). However, the assignments of the cleavage position in Table I could be confirmed in a few cases by mass spectrometry, after elution of peptide fragments from the SDS gels. For the p21N peptide, the exact position of cleavage was determined after extensive tryptic cleavage and mass measurements (by MALDI-TOF MS, ESI-Q-TOF, MS/MS in automatic and manual mode). This analysis unambiguously revealed cleavage after Thr^{181}. Furthermore, the analysis of the MS/MS-sequenced fragmentation pattern of the 170–181 peptide reveals a -CO NH_2 amide in the C terminus instead of COOH (indicated by the fact that there is a deficit of mass of one dalton due to the presence of NH_2 instead of OH; data not shown), as expected according to the mechanism proposed by Berlett and Stadtman (39). Thus, p21N corresponds to the residues 1–181, close to the predicted cleavage point Glu^{183} in the TGES motif, based on the data obtained with Na^+,K^+-ATPase and H^+,K^+-ATPase (19, 31). The complete p21N peptide, as well as other peptides both from the Ca^{2+}-ATPase and from the Na^+,K^+-ATPase, were analyzed by MALDI-TOF MS. This involved the use of a newly developed procedure to elute the fragments from the SDS-PAGE and then exchange the SDS by NaDOC, which is compatible with the MALDI-TOF MS procedure. Examples of spectra of the p21N fragment of Ca^{2+}-ATPase and the corresponding fragment of Na^+,K^+-ATPase are shown in Fig. 6. For p21N, we obtained an average mass of

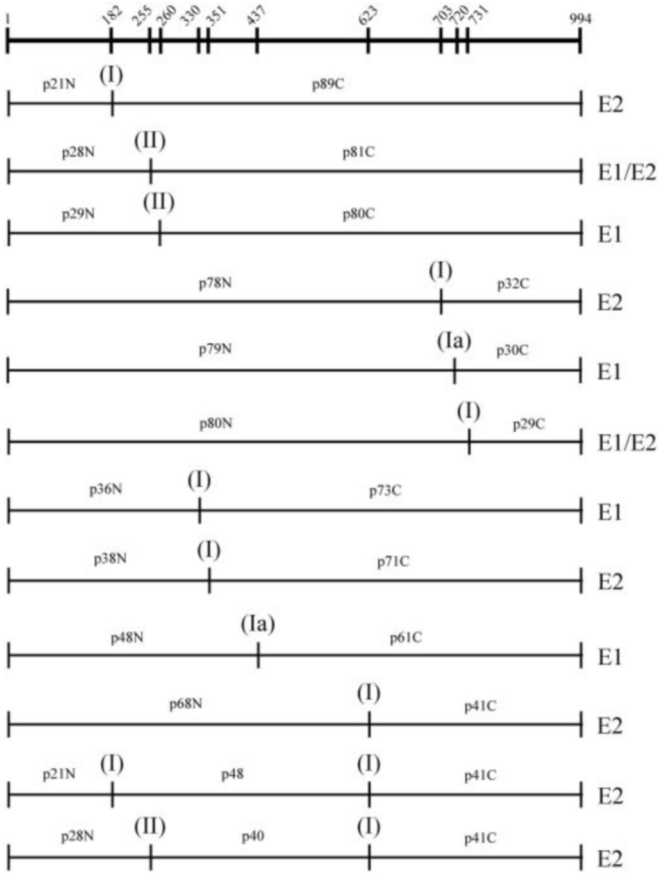

FIG. 5. **A linear map of the various fragments of the Ca^{2+}-ATPase identified after proteolytic attack by Fe^{2+}.** The conditions and appearance of these peptides are detailed in Figs. 1–3 and Table I. Site I is in the cytosolic region, whereas site II is in the membrane interface. *Site Ia* designates the two cleavages that were increased by nucleotide binding (Figs. 3 and 4).

20,421.5 ± 32.2 Da (n = 3), whereas the value expected on the basis of Met^1–Thr^{181}, including acetylation of Met^1, is 20,341 Da. The experimental value is slightly larger than expected, but this can easily be accounted for by a possible oxidation of methionine residues (due to the high H_2O_2 concentration) and/or covalent binding of acrylamide monomers (M_r = 70 Da) in SDS-PAGE gels, which can react with the cysteines of the protein (40). In an attempt to avoid the uncertainty of acrylamide binding, some samples were alkylated with iodoacetamide before analysis (Table II). In the table, we have assumed that alkylation by iodoacetamide occurred on all the cysteine residues, but this could be an overestimate, in particular for membrane proteins (40).[2] Despite these reservations concerning the extent of alkylation and/or possible methionine oxidation, Table II demonstrates excellent agreement between MALDI-TOF MS analysis with the values deduced from the comparative gel electrophoretic analysis. In the case of Na^+,K^+-ATPase, the N termini of two fragments could be determined by Edman degradation (^{214}ESE^{216} C terminus and ^{712}VNDS^{715} C terminus in site I, see Ref. 20). By comparing the theoretical masses of these two fragments and those found by MS, we can estimate, independently, that masses of fragments in the 20–80 kDa range are determined by MALDI-TOF MS with an accuracy of 2–4 residues, respectively.

DISCUSSION

Fe^{2+}-catalyzed oxidation of Ca^{2+}-ATPase results in a number of bands appearing in SDS-PAGE. To identify the points of cleavage, N-terminal sequencing would have been the method of choice, but it is usually not feasible to use Edman degradation after oxidative cleavage due to blocked N termini of cleaved fragments. Therefore we have used alternative methods to identify the cuts as precisely as possible: i) by use of specific antibodies and careful molecular mass estimates based on a number of well known SERCA1a proteolytic fragments from proteinase K or trypsin. Because in this case the migration rate of unknown fragments is compared with that of proteolytic fragments from the same protein, serving as an "ideal standard," the cleavage points can be rather precisely located (probably within 5 residues); ii) molecular masses were independently measured by several mass spectrometry techniques (MALDI-TOF MS, ESI-Q-TOF, MS/MS). In one case (p21N ending at Thr-181), the latter technique allowed us to identify that the C-terminal amino acid is cleaved as an amide; to our knowledge, this is the first time that an oxidative cleavage position could be detected so precisely by mass spectrometry (1 Da). This determination confirms the tendency of oxidative peptide bond cleavage to take place between the amino group and the α carbon on the C-terminal side of the cleaved peptide bond (39). For MALDI-TOF MS analysis, a new protocol was developed to prepare the intact peptides electroeluted from SDS-PAGE (33). This involved a number of steps, in particular a careful removal of SDS after electroelution from the SDS-PAGE by exchange with NaDOC. This method has the important feature of allowing estimation of masses by MALDI-TOF MS of any water-soluble and hydrophobic proteins eluted from SDS-gels. The resulting mass measurements were generally in very good agreement with the cleavage proposed on the basis of the known cleavage sites in Na^+,K^+-ATPase and H^+,K^+-ATPase and the SDS-PAGE calibration mentioned above. From all these data, it has been possible to define with a rather high degree of certainty (2–4 residues in the range 20–80 kDa, respectively) how the cleavage products can be accounted for by cleavage at relatively few positions in a conformation-dependent manner. In relation to the cleavage mechanism, it was noticed previously that a glycine residue is found next to the two exactly known Fe^{2+}-catalyzed cleavage positions of Na^+,K^+-ATPase (TGD**G** ↑ VNDS and T**G** ↑ ES), and we now find this also with Ca^{2+}-ATPase at T ↑ **G**ES. With the greater accuracy of determination by MS, it now seems that this is usually the case (Table I). This generalization helps to locate inexactly known cleavage positions. In addition, the mechanistic implication could be that the side chain of the residue on one or the other side of the glycine makes contact with the bound iron, and the lack of a side chain at the glycine residue creates the space that allows access of the OH radical to the peptide backbone.

The present investigation shows that Fe^{2+}-catalyzed oxidation of Ca^{2+}-ATPase results in a cleavage pattern that in many respects is similar to that of Na^+,K^+-ATPase and H^+,K^+-ATPase (19). In all cases, there is evidence that Fe^{2+} cleavage in the cytosolic domains (site I) is associated with conserved sequences, important for enzyme catalysis. This is especially evident in the E2 conformation in which cleavage localizations, in addition to the phosphorylation site, include the ^{181}TGES^{184} motif in domain A and the ^{623}MTGD^{626} conserved sequence in the P-domain, both of which are involved in ATPase dephosphorylation. Furthermore, in the E2 conformation, there is cleavage at the Mg^{2+} bound at the phosphorylation site, involving the Asp^{703} residue in the TGD^{703}GVNDA region in the C-terminal end of the P-domain (41). As shown in Fig. 7*A* (residues in *green*), all of the aforementioned motifs are assembled around Asp^{351} in the E2(Tg) (1IWO; Ref. 5) structural model. This is also the case for E2(V) (1KJU; Ref. 42) structural

[2] M. le Maire, unpublished data.

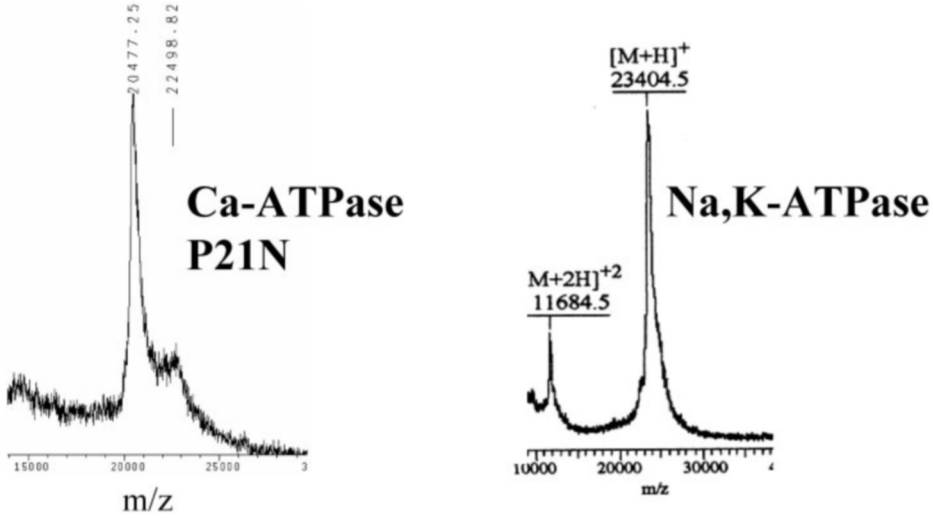

FIG. 6. **MALDI-TOF MS spectra of the p21N fragment of Ca^{2+}-ATPase and analogous fragment of Na$^+$,K$^+$-ATPase.** The fragments were electroeluted from GelCode-stained gels and SDS-exchanged with NaDOC, and MALDI-TOF spectra were recorded as described under "Materials and Methods." See also Table II.

TABLE II

MALDI-TOF MS analysis on fragments of Ca^{2+}-ATPase or Na$^+$,K$^+$-ATPase electroeluted from SDS-gels

The predicted mass is the average mass, including, for Ca^{2+}-ATPase, the N-terminal acetylation. When no alkylation was performed, the MALDI mass is the experimental result without subtraction (but see "Results" concerning possible acrylamide covalent binding), whereas in the case of alkylation, we have assumed complete modification. Thus, we have subtracted 57 times the number of cysteine in this sequence, but we have not taken into account possible methionine oxidation. There is a total of 24 cysteines in Ca^{2+}-ATPase and 23 in Na$^+$,K$^+$-ATPase.

Known (*) or predicted length of fragments	Catalyst, site, domain, conformation	Predicted mass	MALDI mass
		Da	*Da ± S.E.*.
Ca^{2+} ATPase			
(*)^{1}MEAAH . . . T^{181}	Fe^{2+} site I A E2(Tg)	20,381	20,421 ± 32 (n = 3) (no alkylation)
^{1}MEAAH . . . K^{436} ^{437}VGEA-C terminus	ATP·Fe^{2+} site I N E1·ATP·Fe	47,666 61,882	45,835 ± 426 (n = 6) 61,443 (n = 2) (with alkylation)
^{1}MEAAH . . . K^{329}	Fe^{2+} site I P E1Ca$_2$	36,143	35,805 ± 168 (n = 6) (with alkylation)
^{182}GES . . . I^{622}	Fe^{2+} site I A, P E2(Tg)	48,086	48,312 ± 183 (n = 4) (with alkylation)
^{1}MEAAH . . . I^{622} ^{623}MITG-C terminus	Fe^{2+} site I P E2(Tg)	68,440 41,128	70,548 ± 90 (n = 4) (no alkylation) 41,528 ± 58 (n = 4) (no alkylation) 41,963 ± 464 (n = 5) (with alkylation)
Na$^+$ K$^+$ ATPase			
^{1}GRDK . . . G^{213} (*)^{214}ESE-C terminus	ATP·Fe^{2+} site I A E2P	23,421 88,852	23,196 ± 52 (n = 11) 89,814 ± 374 (n = 11) (with alkylation)
^{1}GRDK . . . G^{442} ^{443}DASE-C terminus	ATP·Fe^{2+} site I N E1·ATP·Fe	48,296 64,003	48,562 (n = 2) 64,427 (n = 2) (with alkylation)
^{1}GRDK . . . G^{711} (*)^{712}VNDS-C-terminus	ATP·Fe^{2+} site I P	77,747 34,552	77,762 ± 102 (n = 6) 34,745 ± 109 (n = 8) (with alkylation)
^{283}HFIH-C terminus	E1·ATP·Fe Fe^{2+} site II M E2(K) or E1Na	81,481	81,999 (n = 2) (with alkylation)
^{608}MVTG-C terminus	Fe^{2+} site I P E2(K)	45,614	45,696 ± 124 (n = 5) (with alkylation)

model (data not shown). It has recently been unequivocally shown that Fe^{2+} mimics normal Mg^{2+} binding sites in E2 conformations, leading to production of the TGES and VNDS site I cleavages in Na$^+$,K$^+$-ATPase (18, 43). Our data thus confirm the functional importance and joint involvement of these motifs in the E2 conformation of the ATPase.

Fewer site I cleavages take place in the E1Ca$_2$ (1EUL; Ref. 4) conformation (Fig. 7*B*, residues in *yellow* or *white*), probably as an indication of the absence of cytosolar high affinity binding sites of Fe^{2+} under these conditions. In the E1Ca$_2$ conformation, according to both the x-ray and other structural evidence, the ATPase is in a more open and flexible state than it is in the E2(Tg) (5) and E2(V) (42) state. In agreement with previous evidence on Na$^+$,K$^+$-ATPase (17) and H$^+$-ATPase (22), we have detected a cleavage site in the N-domain probably located near Glu^{439} in the ^{437}VGEATE^{442} region, close to the Thr^{441} Fe^{2+}

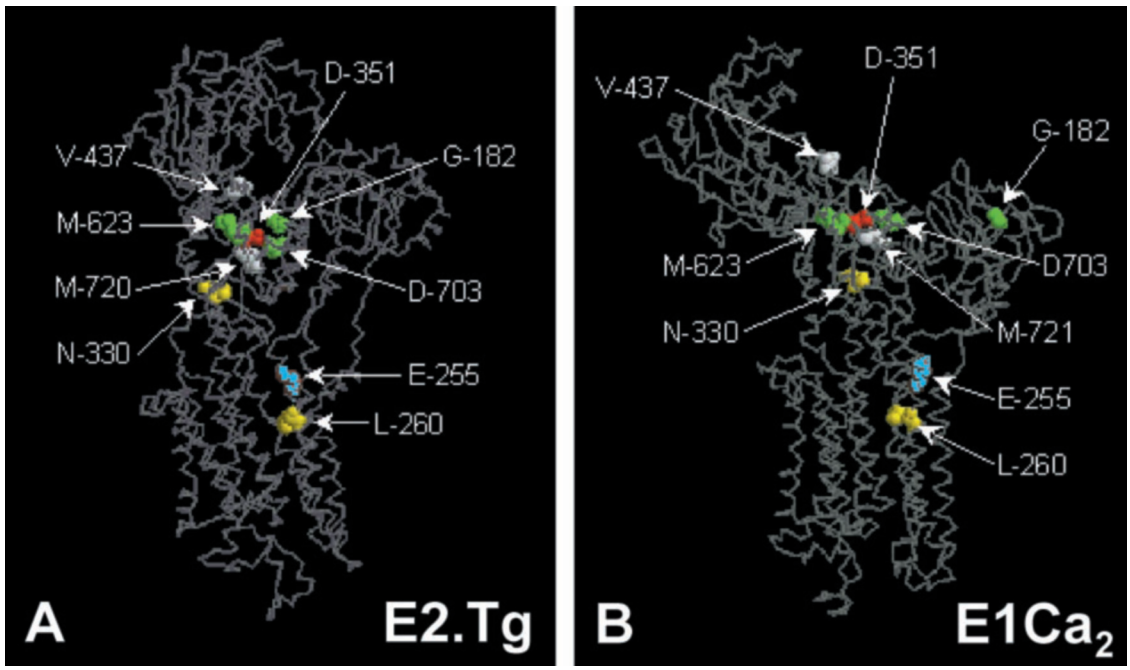

FIG. 7. **Topological location of the Fe^{2+} cleavage points obtained in thapsigargin (*A*) or in Ca^{2+} (*B*), based on structural models of Ca^{2+}-ATPase and the results shown in Table I.** The representations are based on the structures deposited in the Protein Data Bank with the following accession codes: 1IWO (*A*) and 1EUL (*B*). The color code is as follows: *red* for Asp^{351}, *green* for E2(Tg)-specific splits, *yellow* for $E1Ca_2$-specific splits, but *white* for $E1Ca_2$-specific splits enhanced by AMP-PNP. *Blue* indicates Glu^{255}, a split observed both in E2(Tg) and in $E1Ca_2$. Ser^{731}, which is a minor cut and unspecific, is not indicated to avoid overloading.

oxidation site on Ca^{2+}-ATPase identified by Hua *et al.* (21). The formation of this cleavage is enhanced by nucleotide binding, but still, there is evidence from the gels that the cleavage is present in distinct amounts already in the $E1Ca_2$ conformation. This is remarkable since, according to the published 1-EUL x-ray structure (Fig. 7*B*), the residue is about 25 Å removed from the site I center. This finding could suggest a flexible structure of the E1 conformation such that the N-domain can rotate by thermal motion already in the $E1Ca_2$ conformation and, at least momentarily, make contact with the phosphorylation site. Glutaraldehyde cross-linking of residues Lys^{492} and Arg^{678} in the presence of Ca^{2+} and in the absence of ATP also suggest this possibility (44). It has previously been proposed that the Glu^{439} in conjunction with the Asp^{703} residue plays a role in the metal coordination after Mg·ATP binding (18, 43). However, according to recent structural analysis of Ca^{2+}-ATPase in the Ca_2E1·AMP-PCP form, Glu^{439} does not coordinate with Mg^{2+} (6), but in this conformation, in which the N- and P-domains are glued together by bound nucleotide, Glu^{439} is much closer (7–8 Å) to the Mg^{2+} coordinated with Asp^{703} γ-phosphate, Asp^{351}, and Asp^{703} than in the $E1Ca_2$ form (Fig. 8).[3] In addition, Glu^{439} and Asp^{703} in the nucleotide-bound E1 form are located in an internal and solvent-filled cleft formed between the N-, P-, and A-domains. Furthermore, the cleavages at Glu^{443} and Glu^{710} of Na^+,K^+-ATPase always appear or disappear in parallel (18, 31). It is therefore definitely possible that the cleavage in the N-domain could represent the product of close transient associations of the N- and P-domains mediated by the bound AMP-PNP·Fe^{2+} complex, whereas the crystal structure may represent a more stable form in which the N-and P-domains are less close to each other. Interestingly, recent infrared spectroscopy results (10) suggest that nucleotide binding induces a conformation that is characteristic of the bound nucleotide, pointing at a further line of investigation in which future work might be helpful. In any event, the approach of the ATP molecule bound to the N-domain toward the P-

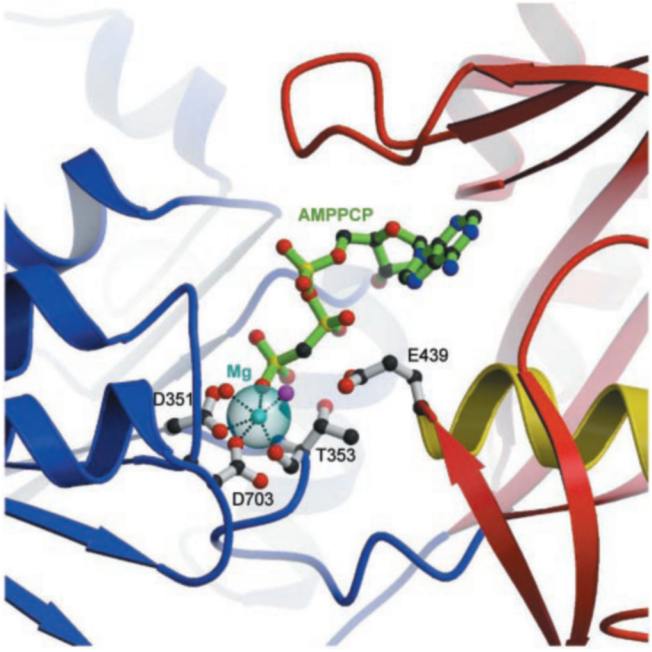

FIG. 8. **Ca^{2+}-ATPase in the Ca_2E1·AMP-PCP form (Sørensen *et al.* (6)) showing the proximity of Glu^{439} to the Mg^{2+} ion binding site.** A magnesium ion is coordinated with the γ-phosphate, Asp^{351}, Asp^{703}, the carbonyl of Thr^{353}, and two water molecules. A solvent-exposed water molecule of the coordination sphere of the magnesium ion is indicated in *magenta*. Glu^{439} does not coordinate with Mg^{2+} but is much closer in this form (7–8 Å) to the Mg^{2+} than in the $E1Ca_2$ form, in line with our proteolysis results obtained by adding AMP-PNP. We expect the Fe^{2+} ion to bind at this site. Note that Glu^{439} is positioned right at the N terminus of a helix, thus with a positive dipole. This might explain the preference of a released hydroxyl radical (perhaps from the position of the magenta water molecule) to attack in that exact region. The figure is provided by courtesy of Poul Nissen.

[3] The same is true concerning the second Mg^{2+} binding site reported by Sørensen *et al.* (6), which is located at a distance of about 5 Å from Glu^{439} but which so far has only been detected corresponding to the phosphorylated transition state.

domain is required for phosphorylation of Asp^{351} to take place, and the parallel N- and P-cleavages can be seen as reflecting this fact. However, it remains uncertain to what extent Mg^{2+} binding extends beyond residues in the phosphorylation motif and Asp^{703}, as demonstrated in the crystal structure of nucleotide-bound Ca^{2+}-ATPase (6) and suggested from site-directed mutagenesis experiments in Na^+,K^+-ATPase (41).

As novel findings, we have detected a cleavage site near ^{720}MGSG^{723} between the P6 and P7 helix of the P-domain. As can be seen from Fig. 7*B*, it is close to the phosphorylation site in the $E1Ca_2$ conformation and, being part of a highly conserved P-type ATPase region, may function as a residue with catalytic properties or participate in the formation of a Mg^{2+} binding site, subject to the same uncertainties as the Glu^{439} residue. In any case, such as that of ^{437}VGEATE^{442} discussed above (Fig. 4), there is, in the presence of AMP-PNP, an increased cleavage of ^{720}MGSG^{723}, suggesting involvement in the Mg·ATP binding process (in Fig. 7, these two sites are colored in *white*). Although the major ATP·Fe^{2+}-induced cleavage site of Na^+,K^+-ATPase is at ^{712}VNDS^{715}, rather than at the homologous ^{727}MGIA^{730}, it was pointed out in Patchornik *et al.* (31) that the broad band is usually resolved as a doublet, with a less prominent fragment 1.5 kDa smaller than the major fragment. Thus, the Na^+,K^+-ATPase may, in fact, be cut at both ^{712}VNDS^{715} and ^{727}MGIA^{730}. The functional importance of Met^{720} has been recently underlined since a mutation in the homologous Met^{731} of the Na^+,K^+-ATPase is associated with familial hemiplegic migraine (45). Finally, we observed weak cleavage sites near ^{731}SEMV^{734}, the occurrence of which appears to be largely conformation-independent, but it is close to a specific K^+ binding site, probably of modulatory importance, that involves Asp^{732}.[4]

Site II cleavages are mainly confined to the ^{255}EFGE^{258} region in the S3 stalk, close to the membrane region. Site II is far removed from the cytosolic site and appears to be subject to cleavage in a largely conformation-independent manner; this site is colored in *blue* in Fig. 7, *A* and *B*. Interestingly, the corresponding region in Na^+,K^+-ATPase (HFIH) has a basic content of amino acid residues. Based on the present data, site II is unlikely just to reflect unspecific binding of Fe^{2+} by complexation with histidine such as could be conceived to be the case on the basis of the Na^+,K^+-ATPase data alone. Possibly, the cleavages in this region could represent binding of Fe^{2+} at a Ca^{2+} pre-binding site suggested to be present somewhere in the M1–3 zone (4, 5, 46–49, 54) to form a gateway for the intramembranous binding and occlusion of Ca^{2+} at Glu^{309} (Ca^{2+} binding site 2). In contrast to findings on Na^+,K^+-ATPase, we could not detect with certainty a cleavage site at the S1/M1 border that could further support this suggestion. However, there is a technical difficulty in assessing this as the homologous site of ^{97}EYVK^{100} in Na^+,K^+-ATPase occurs at a more N-terminal location in Ca^{2+}-ATPase (at ^{48}SLWEL^{52}). A cleavage at this position would produce a very large fragment (104,000 Da), very close to that of the complete enzyme (109,000 Da), and most likely, our SDS-PAGE system would not resolve it. It is interesting to note that the thapsigargin binding site is located near site II (5). Recently, Eckstein-Ludwig *et al.* (50) showed that Artemisinin, a potent antimalaria drug, inhibits PfATP6, an ortholog of SERCA*1a* present in *Plasmodium falciparum*, probably by binding at the same site as thapsigargin. The inhibition was found to be dependent upon the presence of Fe^{2+} ions and thus could be prevented by the presence of deferoxamine. The basis for the Artemisinin effect appears to be that an endoperoxide bridge generates short-lived radicals in the presence of Fe^{2+}. This emphasizes the importance of oxidative stress in the cellular environment and opens new perspectives on Fe^{2+}-oxidative damages.

[4] T. L-M. Sørensen, J. V. Møller, and P. Nissen, unpublished observations.

Acknowledgments—We are very grateful to Prof. P. Nissen for preparing Fig. 8, and we thank Prof. Nissen and Drs. P. Champeil, P. Falson, and G. Lenoir for many helpful suggestions. We thank Dr. B. Juul and M. A. Hoste for help in the initial part of this work.

REFERENCES

1. Axelsen, K. B., and Palmgren, M. G. (1998) *J. Mol. Evol.* **46,** 84–101
2. Møller, J. V., Juul, B., and le Maire, M. (1996) *Biochim. Biophys. Acta* **1286,** 1–51
3. Brandl, C. J., Green, N. M., Korczak, B., and MacLennan, D. H. (1986) *Cell* **44,** 597–607
4. Toyoshima, C., Nakasako, M., Nomura, H., and Ogawa, H. (2000) *Nature* **405,** 647–655
5. Toyoshima, C., and Nomura, H. (2002) *Nature* **418,** 605–611
6. Sørensen, T. L-M., Møller, J. V., and Nissen, P. (2004) *Science* **304,** 1672–1675
7. Andersen, J. P. (1995) *Biosci. Rep.* **15,** 243–261
8. Vilsen, B. (1995) *Acta Physiol. Scand.* **154,** Suppl. 624, 1–146
9. Bigelow, D. J., and Inesi, G. (1992) *Biochim. Biophys. Acta* **1113,** 323–338
10. Liu, M., and Barth, A. (2003) *J. Biol. Chem.* **278,** 10112–10118
11. Green, N. M., and MacLennan, D. H. (2002) *Nature* **418,** 598–599
12. Lee, A. G. (2002) *Biochim. Biophys. Acta* **1565,** 246–266
13. Scarborough, G. A. (2002) *J. Bioenerg. Biomembr.* **34,** 235–250
14. Jorgensen, P. L., Hakansson, K. O., and Karlish, S. J. D. (2003) *Annu. Rev. Physiol.* **65,** 817–849
15. Stokes, D. L., and Green, N. M. (2003) *Annu. Rev. Biophys. Biomol. Struct.* **32,** 445–468
16. Toyoshima, C., and Inesi, G. (2004) *Annu. Rev. Biochem.* **73,** 269–292
17. Karlish, S. J. D. (2003) *Ann. N. Y. Acad. Sci.* **986,** 39–49
18. Strugatsky, D., Gottschalk, K. E., Goldshleger, R., Bibi, E., and Karlish, S. J. D. (2003) *J. Biol. Chem.* **278,** 46064–46073
19. Shin, J. M., Goldshleger, R., Munson, K. B., Sachs, G., and Karlish, S. J. D. (2001) *J. Biol. Chem.* **276,** 48440–48450
20. Goldshleger, R., and Karlish, S. J. D. (1997) *Proc. Natl. Acad. Sci. U. S. A.* **94,** 9596–9601
21. Hua, S., Inesi, G., Nomura, H., and Toyoshima, C. (2002) *Biochemistry* **41,** 11405–11410
22. Valiakhmetov, A., and Perlin, D. S. (2003) *J. Biol. Chem.* **278,** 6330–6336
23. de Meis, L., and Hasselbach, W. (1971) *J. Biol. Chem.* **246,** 4759–4763
24. Champeil, P., Guillain, F., Vénien, C., and Gingold, M. P. (1985) *Biochemistry* **24,** 69–81
25. Sagara, Y., Fernandez-Belda, F., de Meis, L., and Inesi, G. (1992) *J. Biol. Chem.* **267,** 12606–12613
26. Henao, F., Orlowski, S., Merah, Z., and Champeil, P. (1992) *J. Biol. Chem.* **267,** 10302–10312
27. Møller, J. V., Lind, K. E., and Andersen, J. P. (1980) *J. Biol. Chem.* **255,** 1912–1920
28. Shevchenko, A., Wilm, M., Vorm, O., and Mann, M. (1996) *Anal. Chem.* **68,** 850–858
29. Jørgensen, P. L. (1988) *Methods Enzymol.* **156,** 29–43
30. Goldshleger, R., and Karlish, S. J. D. (1999) *J. Biol. Chem.* **274,** 16213–16221
31. Patchornik, G., Goldshleger, R., and Karlish, S. J. D. (2000) *Proc. Natl. Acad. Sci. U. S. A.* **97,** 11954–11959
32. Capasso, J. M., Hoving, S., Tal, D. M., Goldshleger, R., and Karlish, S. J. D. (1992) *J. Biol. Chem.* **267,** 1150–1158
33. Mehlman, T., Benjamin, M., Merhav, D., Osman, F., Ben-Asouli, Y., Goldshleger, R., Karlish, S., and Shainskaya, A. (2002) *Proceedings of the 50th Conference of American Society for Mass Spectrometry*, June 2–6, 2002, Orlando, FL, American Society for Mass Spectrometry, Orlando, FL
34. Jensen, O. N., Podtelejnikov, A., and Mann, M. (1996) *Rapid Commun. Mass Spect.* **10,** 1371–1378
35. Juul, B., Turc, H., Durand, M. L., Gomez de Gracia, A., Denoroy, L., Møller, J. V., Champeil, P., and le Maire, M. (1995) *J. Biol. Chem.* **270,** 20123–20134
36. le Maire, M., Lund, S., Viel, A., Champeil, P., and Møller, J. V. (1990) *J. Biol. Chem.* **265,** 1111–1123
37. Møller, J. V., Ning, G., Maunsbach, A. B., Fujimoto, K., Asai, K., Juul, B., Lee, Y.-J., Gomez de Gracia, A., Falson, P., and le Maire, M. (1997) *J. Biol. Chem.* **272,** 29015–29032
38. Tam, J. P. (1988) *Proc. Natl. Acad. Sci. U. S. A.* **85,** 5409–5430
39. Berlett, B. S., and Stadtman, E. R. (1997) *J. Biol. Chem.* **272,** 20313–20316
40. le Maire, M., Deschamps, S., Møller, J. V., Le Caer, J. P., and Rossier, J. (1993) *Anal. Biochem.* **214,** 50–57
41. Jorgensen, P. L., Jorgensen, J. R., and Pedersen, P. A. (2001) *J. Bioenerg. Biomembr.* **33,** 367–377
42. Xu, C., Rice, W. J., He, W., and Stokes, D. L. (2002) *J. Mol. Biol.* **316,** 201–211
43. Patchornik, G., Munson, K., Goldshleger, R., Shainskaya, A., Sachs, G., and Karlish, S. J. D. (2002) *Biochemistry* **41,** 11740–11749
44. McIntosh, D. B. (1992) *J. Biol. Chem.* **267,** 22328–22335
45. Vanmolkot, K. R., Kors, E. E., Hottenga, J. J., Terwindt, G. M., Haan, J., Hoefnagels, W. A., Black, D. F., Sandkuijl, L. A., Frants, R. R., Ferrari, M. D., and van den Maagdenberg, A. M. (2003) *Ann. Neurol.* **54,** 360–366
46. Lee, A. G., and East, J. M. (2001) *Biochem. J.* **356,** 665–683
47. Andersen, J. P., Sørensen, T. L.-M., Povlsen, K., and Vilsen, B. (2001) *J. Biol.*

Chem. **276,** 23312–23321
48. Einholm, A. P., Vilsen, B., and Andersen, J. P. (2004) *J. Biol. Chem.* **279,** 15888–15896
49. Inesi, G., Ma, H., Lewis, D., and Xu, C. (2004) *J. Biol. Chem.*, **279,** 31629–31637
50. Eckstein-Ludwig, U., Webb, R. J., Van Goethem, I. D., East, J. M., Lee, A. G., Kimura, M., O'Neill, P. M., Bray, P. G., Ward, S. A., and Krishna, S. (2003) *Nature* **424,** 957–961
51. Imamura, Y., and Kawakita, M. (1989) *J. Biochem.* (*Tokyo*) **105,** 775–781
52. Lesniak, W., Modyanov, N., and Chiesi, M. (1994) *Biochemistry* **33,** 13678–13683
53. Castilho, R. F., Carvalho-Alves, P. C., Vercesi, A. E., and Ferreira, S. T. (1996) *Mol. Cell. Biochem.* **159,** 105–114
54. Clausen, J., and Andersen, J. P. (2003) *Biochemistry* **42,** 2585–2594